CROP WIND ENERGY EXPERIMENT (CWEX)

Observations of Surface-Layer, Boundary Layer, and Mesoscale Interactions with a Wind Farm

BY DANIEL A. RAJEWSKI, EUGENE S. TAKLE, JULIE K. LUNDQUIST, STEVEN ONCLEY, JOHN H. PRUEGER, THOMAS W. HORST, MICHAEL E. RHODES, RICHARD PFEIFFER, JERRY L. HATFIELD, KRISTOPHER K. SPOTH, AND RUSSELL K. DOORENBOS

CWEX demonstrates the importance of collecting field measurements within a wind farm to facilitate basic understanding of the three-way interactions among wind energy, meteorology, and crop agriculture.

The U.S. Department of Energy (DOE) has outlined a scenario describing how wind power can be a major contributor to meet future U.S. renewable energy needs (U.S. DOE 2008). The *20% Wind Energy by 2030* report outlines steps for achieving 20% of the nation's electrical energy from wind by 2030, a tenfold increase from the current level of 2% (AWEA 2011). Most of the richest land-based domestic resources of wind power in the United States are located in the central United States (North and South Dakota, Minnesota, Iowa, Illinois, Nebraska, Kansas, Oklahoma, Texas). Therefore, the DOE 20% by 2030 scenario will likely create additional interest in expanding the number of wind farms in this region. These states also produce most of the nation's wheat and corn for food, livestock feed, and biofuel. Iowa alone accounts for 19% of the nation's production of corn as well as 15% of soybean (USDA 2012). Much of this production is on the same land now being considered for wind farms.

While the collocation of wind farms with intensively managed agricultural production is possible, it leads to physical interactions between two otherwise separate economic systems. Crop selection and management determines surface drag and fluxes that influence hub-height wind speeds. By contrast, turbine-generated changes in mean wind, pressure, and turbulence may influence fluxes of

AFFILIATIONS: RAJEWSKI—Department of Geological and Atmospheric Sciences, Iowa State University, Ames, Iowa; TAKLE, SPOTH, AND DOORENBOS—Department of Agronomy, Iowa State University, Ames, Iowa; LUNDQUIST—Department of Atmospheric and Oceanic Sciences, University of Colorado, Boulder, and National Renewable Energy Laboratory, Golden, Colorado; ONCLEY AND HORST—National Center for Atmospheric Research, Boulder, Colorado; PRUEGER, PFEIFFER, AND HATFIELD—National Laboratory for Agriculture and the Environment, Ames, Iowa; RHODES—Aerospace Engineering Sciences, University of Colorado, Boulder, Colorado
CORRESPONDING AUTHOR: Daniel A. Rajewski, Iowa State University, 3132 Agronomy, Ames, IA 50011
E-mail: drajewsk@iastate.edu

The abstract for this article can be found in this issue, following the table of contents.
DOI:10.1175/BAMS-D-11-00240.1

In final form 18 September 2012

heat, moisture, and CO_2 that are of vital importance to biophysical crop processes. Because multimegawatt turbines and their access roads require less than half an acre of land, farmers often continue to graze livestock and farm crops right up to turbines' bases (UCS 2011). However, because the wakes of wind turbines are known to persist up to 15 rotor diameters *D* downwind of a turbine (Meyers and Meneveau 2012), differences in microclimate may extend well beyond the wind turbines' small footprint on the landscape. As a result, some agronomists and producers have questioned whether the atmospheric impacts of wind turbines may also influence the biological productivity of the surrounding crops (E. Takle 2009, personal communication). Therefore, our goal for the Crop Wind Energy Experiment (CWEX) is to develop a basic understanding of how this land use collocation changes both the energy and crop production systems that contribute to the nation's food and energy security needs.

Originally, CWEX was launched to address the following four agronomic questions:

1) Do turbines create measureable changes in microclimate over crops?
2) If question 1 is true, then are these changes large enough to produce measureable influences on plant growth?
3) If questions 1 and 2 are true, then are these changes sufficient to have measureable impact on yield?
4) Do agricultural cropping and surface management practices have a measureable impact on wind energy production?

For this study we will report on the first of these questions and the other three will be topics of future CWEX experiments.

Two summer measurement campaigns were conducted to observe surface and elevated meteorological conditions in a wind farm collocated with agricultural fields. In the summer 2010 experiment, designated CWEX-10, the National Laboratory for Agriculture and the Environment (NLAE) deployed four flux stations in cornfields within a wind farm in central Iowa. The University of Colorado conducted upper-air observations for a portion of the summer. The second summer measurement period, CWEX-11, coincided with a 10-week Iowa State University summer program of the National Science Foundation Research Experiences for Undergraduates (REU) in Wind Energy Science, Engineering, and Policy (WESEP). In support of the WESEP REU, the Earth Observing Laboratory (EOL) of the National Center for Atmospheric Research (NCAR) provided an educational deployment of instruments to the wind farm consisting of four surface flux stations, and included operational support and data archives. Iowa State University (ISU) provided two flux stations for CWEX-11. The National Renewable Energy Laboratory and the University of Colorado provided two wind-profiling lidars to observe wind and turbulence profiles during CWEX-11.

Numerous discussions with representatives from the agricultural, wind energy, and boundary layer meteorology communities about the summer field measurement campaigns have affirmed that the extension of CWEX to a more comprehensive field program offers a unique opportunity to create a deeper understanding of the range of basic and applied science issues.

The "Site description" section describes the CWEX site, highlighting its use for current and future field campaigns to address these critical questions. The experimental design and instrumentation are described in the "CWEX measurement design" section. An analysis of surface flux differences is presented in the "Detection of turbine-induced surface flux differences" section, and a case study of the differences in fluxes and in wind and turbulence profiles is in the "Turbine wake influences on wind and turbulence profiles: A case study, night of 16–17 July 2011." In the "Turbine influences on fluxes of heat and carbon dioxide" section, we demonstrate the potential influence of turbines on daytime crop–canopy fluxes of heat and carbon dioxide. Last, in the "Remaining science questions and future campaigns" section, we present an expanded list of science questions and prospects for future campaigns and solicit engagement from the academic, national laboratory, and private sector segments of the agronomic, wind energy, and boundary layer/mesoscale meteorology communities.

SITE DESCRIPTION. The CWEX experiments were conducted within a 200-turbine (1.5-MW rated power) wind farm in central Iowa. The wind farm features General Electric (GE) 1.5-MW super-long extended (SLE) model turbines (rated wind speed of 14 m s^{-1}) with hub heights of 80 m and rotor diameters of 74 m for the southernmost 100 turbines and GE 1.5-MW extra-long extended (XLE) model turbines (rated wind speed of 11.5 m s^{-1}) with rotor diameters of 77 and 82.5 m for the northern 100 turbines. Additional turbine specifications are available from GE and in its brochure on 1.5-MW wind turbines (General Electric Energy 2009). The land generally is flat, with less than

a 0.5° slope from southwest to northeast. Crops in the wind farm were a patchwork of mostly corn and soybeans, with some wetland and lower terrain at the southern edge of the wind farm. Measurements were taken at the southwest edge of the farm, as shown in Fig.1, to explore crop–turbine–boundary layer interactions in the vicinity of the leading line of turbines, designated as the B turbine line, for the predominant wind direction (south to south-southeast), in mid- to late summer. Climatological wind roses for the nearby Marshalltown, Iowa, airport document prevailing winds for the months of January (Fig. 2a) and July (Fig. 2b). Additional wind roses are available from the Iowa Environmental Mesonet (http://mesonet.agron.iastate.edu/sites/windrose.phtml?network=IA_ASOS). Within the study area is a second line of turbines, designated as the A turbine line, located 1.7 km to the north of the leading line, and a third line, designated as the C turbine line, is located 1.8 km southeast of the turbine line of our CWEX-10/CWEX-11 measurement site.

For both CWEX-10 and CWEX-11, measurements were collected above and within a corn canopy. At the start of each experiment (late June), the crop height was about 1.5 m, and by the second to third week of July the canopy reached its maximum height near 2.8 m. Roughness length varied from 0.05 to approximately 0.4 m for neutral stratification conditions, which closely follows the parameterization of one-tenth the canopy height (Campbell and Norman 1998).

CWEX MEASUREMENT DESIGN. To address our initial question, CWEX-10 was designed to examine differences in surface fluxes and mean variables at several locations in the vicinity of one line of turbines. Several offshore studies suggest that turbine wake interaction with the surface would be detected beyond 5–10*D* downwind from the turbines (e.g., Barthelmie et al. 2010). Preliminary profile measurements of temperature and 2-m wind speed above a soybean canopy were taken at the wind farm around the A and B lines of turbines in 2009. One mast was held stationary at a distance of 3–4*D* upwind of the line of turbines and depending on the wind direction the other mast was moved every 20 min at intervals of 1D downstream of the turbine line. Differences in surface mean wind speed, turbulence intensity, and thermal instability were observed at a few locations within 2–3*D* behind the turbines; however, impacts were diminished in the 5–7*D* range and the results from these simple studies were the impetus for the larger experiments conducted in CWEX-10/CWEX-11.

For CWEX-10, four surface flux stations, designated NLAE 1–4 in Fig. 1, were provided by

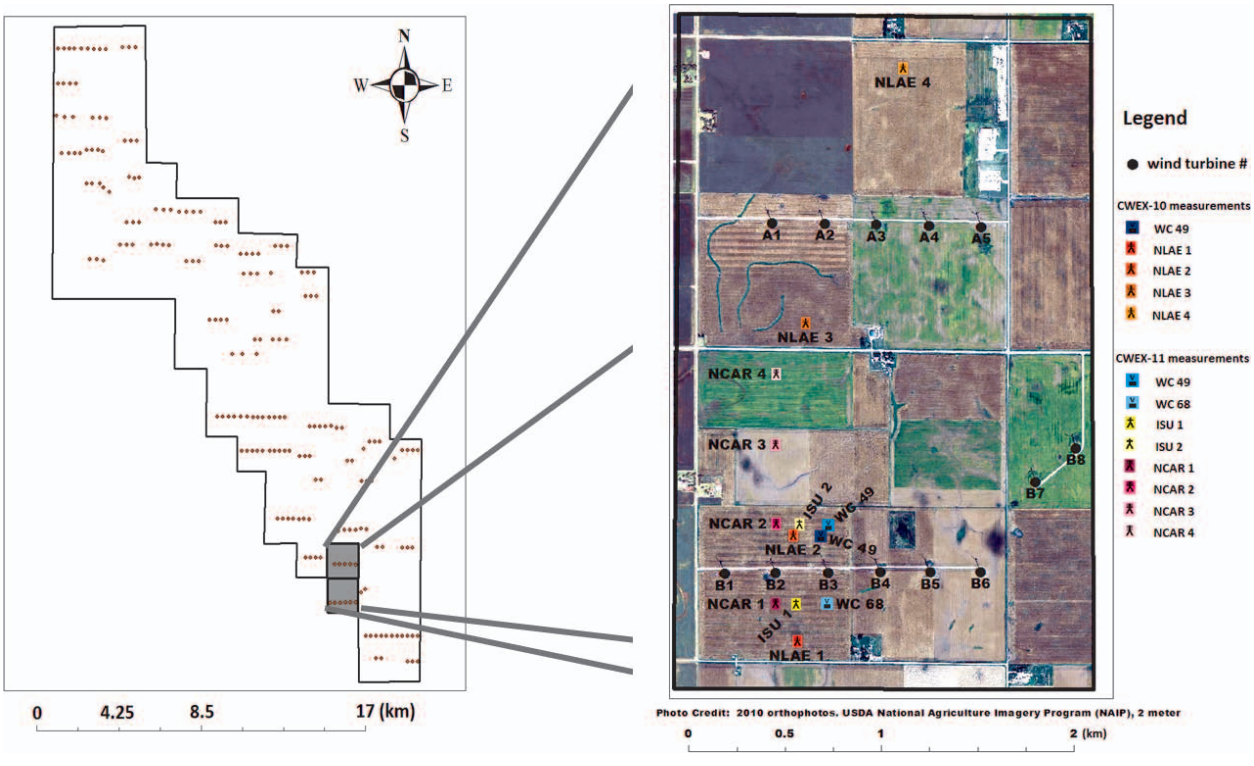

Fig. 1. Overlay of the wind farm boundaries with an expanded view of the measurement locations for CWEX-10 and CWEX-11.

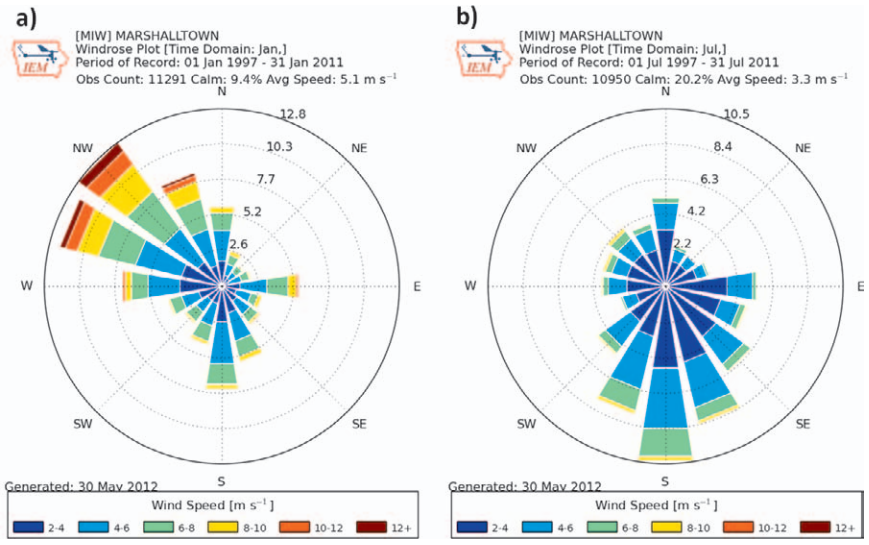

Fig. 2. Climatological 10-m wind roses of the Marshalltown airport for the months of (a) Jan and (b) Jul.

the National Laboratory for Agriculture and the Environment. The upwind flux tower in CWEX-10 was placed about 4.5*D* south of the B turbine line to measure characteristics of the undisturbed flow of the prevailing southerly winds. A second flux tower sampled a near-wake position about 2.5*D* north of the B turbine line. The third flux tower was located 17*D* from the B turbine line for observations at a "far wake" location. A fourth flux tower was placed north of the A turbine line about 35*D* downstream of the B turbine line to capture the influence of wakes from two lines of turbines. The significant variability of turbine wakes observed in CWEX-10 demonstrated the need for detailed measurements of surface flux differences at closer distances from the leading line of turbines. Therefore, in CWEX-11, more flux towers were deployed closer to the B turbine line. The upwind reference tower (NCAR 1) was placed 2.0*D* south of turbine B2. The northerly (downwind) flux towers (NCAR 2–4) were placed at 3.5*D*, 9*D*, and 14*D*, respectively, north of turbine B2. Two additional flux towers, designated as ISU 1 and ISU 2, were placed north and south of the midpoint between turbines B2 and B3, at approximately 2.0*D* upwind and 3.5*D* downwind, respectively.

From data collected by the Windcube (WC) lidar (version 1, manufactured by Leosphere and NRG Systems, Inc.) that was deployed for two weeks in CWEX-10, we learned that sufficient particulate loading within the boundary layer in this location enabled high-quality wind and turbulence profiles to be collected as a complement to surface-based measurements. The lidar could "see" to 120 m above the surface over 95% of the time (Aitken et al. 2012). As a result, two LIDARs, designated as WC 68 and WC 49, were deployed in CWEX-11 to observe wind and turbulence profiles at approximately 2.0*D* south and 3.5*D* north, respectively, of turbine B3.

Flux stations in CWEX-10 and CWEX-11 had similar instrumentation (e.g., sonic and cup anemometers), but not all measurements were collected at identical heights or with the same type of sensor. Table 1 provides lists of the key instrumentation used in the two years of the study.

Data from the sonic anemometers, krypton hygrometers, and gas analyzers were collected at 20 Hz, whereas other flux station sensors sampled every 1 Hz, and the wind and turbulence profiles were collected every 0.5 Hz. CWEX-10 was conducted from 27 June to 7 September 2010. We report herein only measurements taken when the turbines were operational. In CWEX-11, flux measurements and wind profiles were archived for the period 29 June–16 August 2011.

One lesson learned from CWEX-10/CWEX-11 is the inherent variability of the cropland within the wind farm, even in the rather featureless terrain of CWEX, due to variations in soil type, drainage quality, and land management practices (tillage, row spacing, cultivar type, planting date, and chemical applications); these factors influence crop growth and therefore fluxes of heat, moisture, CO_2, and momentum within and above the crop canopy. Direct comparison of CWEX-10 and CWEX-11 differences in the flux data also are complicated by the contrasts in growing season weather. Conditions during CWEX-10 were abnormally wet, whereas the summer of 2011 was much drier. No clear change in crop roughness was observed from the two distinctly different growing seasons. The following section provides the results of surface fluxes from CWEX-10, in which similarities were observed in the data from CWEX-11.

DETECTION OF TURBINE-INDUCED SURFACE FLUX DIFFERENCES.

We used the wind direction from the near-wake flux tower (NLAE

2 in CWEX-10 and NCAR 2 in CWEX-11) to distinguish between wake and nonwake periods (periods when an individual wake from turbine B2 or B3 was most likely overhead of the flux station). For hub-height wind speeds below 15 m s^{-1}, Barthelmie et al. (2010) observed that as wakes advect downwind, they tend to expand by 5° within the first 10*D* downwind. The same procedure also was applied in CWEX-11 for determining the turbine B3 wake for southerly flow and westerly flow nonwake periods for the lidar data. The wind directions that represent the influence of wake for NLAE 2, NCAR 2, and WC 49 are marked on the upwind wind roses for NLAE 1, NCAR 1, and WC 68, respectively (Figs. 3a–c). The plots demonstrate the importance of measuring wind speed and direction at multiple elevations near the turbines, especially under thermally stratified nighttime conditions, when the turbines are operating within or underneath a low-level jet environment that includes significant speed and directional shear.

To investigate the flux differences attributable to the turbine B2 in 2010, we considered the wind direction window 189°–221° to give a wake over the NLAE stations, for which we had a total of four hundred and twenty 15-min observations. These were compared to observations with westerly flow (248°–282°) that gave no wake over the NLAE stations, for which we had 413 observations. We also present a south-southeast flow condition (151°–189°) for which NLAE 2 was between the wakes of turbines B2 and B3. For this wind direction window, we had 574 observations. The differences in conditions between flux towers north and south of the B turbine line were compared for daytime and nighttime conditions. We used the common scaling of thermal stability (z/L_0) at the reference flux tower, where z is the height of the

Table 1. Instrumentation type, sensor height, and location for flux stations operating during CWEX-10 and CWEX-11. More detailed specifications of each sensor can be found in the footnotes.

Sensor type	Height above ground (m) CWEX-10	Location for CWEX-10	Height above ground (m) for CWEX −11	Location for CWEX-11
Sonic anemometer[a]	6.5	NLAE 1–4	4.5	NCAR 1–4 ISU 1–2
Net radiometer[b]	6.5	NLAE 1–2	4.5	ISU 1–2
Gas analyzer[c]	6.5	NLAE 1–2	4.5	NCAR 1,3 ISU 1
Cup/prop anemometer[d]	9.0	NLAE 1–4	10 8, 3	NCAR 1–4 ISU 1–2
Temperature–relative humidity probe[e]	5.3, 9.0	NLAE 1–4	10, 2 8, 3, 1	NCAR 1–4 ISU 1–2
Tipping bucket[f]	5.2	NLAE 1–4	3.3	ISU 1–2
Air pressure[g]	6.5	NLAE 1–2	2 4.5	NCAR 1–4 ISU 1
Leaf wetness[h]			2 1.7	NCAR 1 ISU 1–2

[a] CSAT3 (Campbell Scientific Inc.); possible 0.6°C warm bias at NLAE 1.

[b] CNR 1 and CNR 4 (Kipp and Zonen) for ISU 1–2; Q7.1 REBS (REBS, Inc.) for NLAE 1, 2.

[c] LI-7500 (LI-COR Biosciences) for NLAE 1, 2 and NCAR 1, 3; EC-150 (Campbell Scientific, Inc.) for ISU 1; H_2O flux measured with Krypton hygrometer at NCAR 2, 4.

[d] 03101 Wind Sentry (Campbell Scientific Inc.) for NLAE 1–4 and ISU 1–2; 05103 Wind Monitor (R. M. Young) for NCAR 1–4.

[e] HMP40/45C (Campbell Scientific Inc.) for NLAE 1–4 and ISU 1, 2; HMP50 (Campbell Scientific Inc.) for ISU 1, 2; NCAR SHT-75 thermohygrometer with aspiration systems for NCAR 1–4.

[f] TE-525 (Texas Electronics).

[g] LI-7500 for NLAE 1, 2; EC-150 for ISU 1; PTB 220 (Vaisala) for NCAR 1–4.

[h] Leaf wetness sensor (Decagon Devices, Inc.); measured on the NCAR 1 tower and in the canopy.

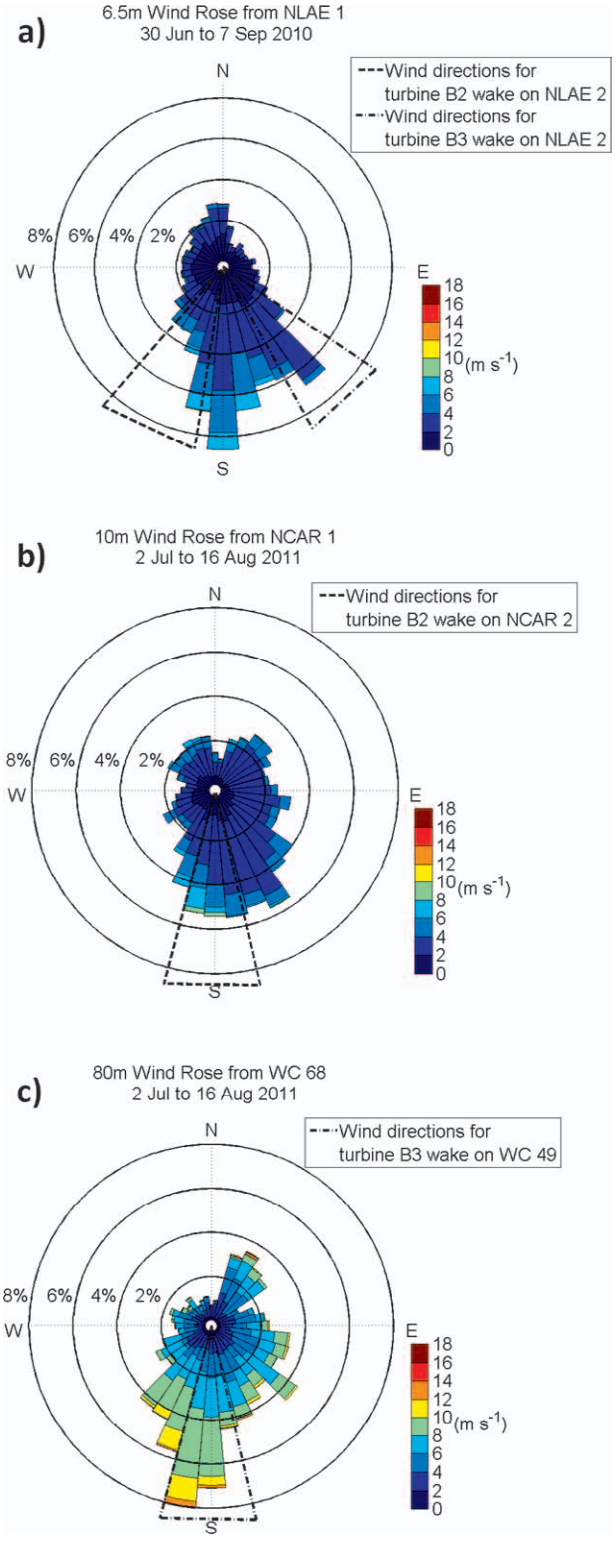

Fig. 3. Wind roses for (a) CWEX-10 6.5-m winds at the reference flux tower (NLAE 1), (b) CWEX-11 10-m winds at the reference flux tower (NCAR 1), and (c) CWEX-11 80-m winds from the upwind Windcube (WC 68). Dashed lines denote wind directions for turbine wakes on downwind stations.

sonic anemometer (6.5 m in CWEX-10 and 4.5 m in CWEX-11). The Obukhov length at the reference flux tower L_0 is defined following Stull (1988):

$$L_0 = \frac{-\overline{\theta}_v u_*^3}{kg(w'\theta_v')_s},$$

and k is von Karman's constant (0.4), u_* is the friction velocity, $\overline{\theta}_v$ is the surface virtual potential temperature, and $(\overline{w'\theta_v'})_s$ is the surface moist sensible heat flux defined over a 15-min averaging period.

Differences between the reference station (NLAE 1) and the flux towers (NLAE 2–4) north of the B turbine line demonstrate the influence of turbines at 6.5 m in the turbulence and sensible heat fluxes and at 9 m for the mean wind speed and air temperature (Fig. 4). We calculate a normalized wind speed difference,

$$\left(\frac{u-u_o}{u_o}\right),$$

and TKE difference,

$$\left(\frac{\mathrm{TKE}-\mathrm{TKE}_o}{\mathrm{TKE}_o}\right),$$

with respect to the undisturbed upwind reference speed, u_o, and turbulence kinetic energy, TKE_o, at the same height according to the analysis methods for simulating shelterbelt wind break flow in Wang and Takle (1995). Tables 2–5 quantify the mean and spread of the normalized wind speed, TKE, air temperature, and the sensible heat flux, respectively, for each stability class and flux station north and south of the B line of turbines for flow from the west (nonwake), southwest (B2 wake), and the south-southeast (flow between the wakes of turbines B2 and B3). We classify each set of differences into three categories of the reference stability: unstable ($z/L_0 < -0.05$), neutral ($-0.05 \le z/L_0 \le 0.05$), and stable ($z/L_0 > 0.05$). Notable values are marked with an asterisk in Tables 2–5.

The nonwake westerly flow in Figs. 4a,d shows considerable scatter in the wind speed and TKE for all stability conditions, but the overall mean difference is near zero at the NLAE 2 and NLAE 3 flux towers. For this (westerly) flow direction, the data from NLAE 4 should be considered inconclusive, since they may in some cases be influenced by the four turbines to the west of the A line (shown in the wind farm layout in Fig. 1).

For a narrow window of southwesterly flow, the wake of turbine B2 is overhead our line of flux

stations. Wind speeds are reduced (by 10%–40%) in neutral to slightly unstable conditions at NLAE 2 and NLAE 4, but this effect is negligible at NLAE 3 (Fig. 4b). The difference in wind speed between NLAE 2 and NLAE 1 reveals a slowdown in the near wake of the turbine, whereas at NLAE 3 there is a slight speed recovery, presumably because higher speed air from above has begun to replenish the near-turbine deficit. At NLAE 4 there is an aggregated influence from both the B turbine line and the A turbine line. The surface-level wind speed reductions we report are in agreement with daytime velocity deficits at tall tower masts for an isolated turbine or groups of turbines in onshore coastal studies (e.g., Högström et al. 1988; Magnusson and Smedman 1994). For stable flow the number of observations is low, but a relatively high percentage of these observations show a speedup at all flux towers north of the B line of turbines. TKE measurements (Fig. 4e) for the nighttime B2 wake condition show substantial enhancement at all stations downwind of B2, but we note high variability in the normalized TKE (Table 3). For the daytime flow, by contrast, the characteristically large TKE at the reference station is enhanced only modestly (<20%) by the turbine as measured at downwind stations.

For south-southeast winds the NLAE 2 flux station is between the wakes of turbines B2 and B3. As shown in Fig. 4c, the northern two flux towers detect higher nighttime overspeeding (e.g., speeds downwind of the turbine being larger than the upwind reference speed) than at NLAE 2, which demonstrates the expanding influence of multiple wakes beyond 10*D* from the B line of turbines. Under stably-stratified nighttime conditions, this localized jet is not rapidly dissipated by turbulent exchange, whereas more turbulent neutral conditions suppress the tendency for wind speed enhancement. We revisit nighttime overspeeding in the "Turbine wake influences on wind and turbulence profiles: A case study, night of 16–17 July 2011" section. There are clear effects of enhanced TKE (4–5 times TKE_o) at NLAE 4 from the combined influence of the A and B lines of turbines. NLAE 3 has higher TKE (2.5 times TKE_o) than the near-wake location at NLAE 2, which we attribute to the aforementioned expansion of multiple wakes several tens of diameters downstream from the B line. Turbulence at NLAE 2 is slightly enhanced, likely due to the overspeeding at this location. Although Fig. 4f demonstrates substantial differences in the normalized TKE for stable flow at all three stations downwind of the B turbine line, we detect high variability among the individual cases. TKE is enhanced at the northern flux stations when the upstream turbulence is very low.

We observed a slight cooling (<0.75°C) at 9 m during the daytime for the two northernmost stations in the southwest B2 wake and south-southeast B2 and B3 gap conditions (Figs. 4h,i), but temperature contrasts between NLAE 2 and NLAE 1 are generally less than 0.5°C as are all differences in the daytime westerly case (Fig. 4g). For nighttime periods the scatter of temperature differences is high for west wind conditions, and a lack of data prevents analysis of temperature impacts for the B2 wake case. However, for south-southeast winds we anticipate wakes from turbines B2 and B3 to spread out and reach the surface somewhere near NLAE 3. At the northernmost flux station (NLAE 4), we see a compounding influence of both B and A turbines to produce several individual periods with a significant warming of 1.0°–1.5°C. Although the variability is high (Table 4), we observe nighttime warming at NLAE 4, similar to that reported at the downwind edge of the San Gorgoino wind farm and statistically analyzed in comparison to airport data by Baidya Roy and Traiteur (2010).

In our report of sensible heat flux differences, we caution that the fluxes are derived from the sonic temperature without making a correction for the humidity in the air. Moisture correction was not possible at NLAE 3 and NLAE 4, since these stations did not measure H_2O and CO_2 and therefore could not record fluxes of these constituents. The "uncorrected" sensible heat flux shows significant scatter of daytime differences for all three directional categories (Figs. 4j–l). For stable conditions we would expect turbine-generated turbulence to be enhancing downward heat flux if the turbine wake is intersecting with the surface. Overall, the data do not show a systematic and significant influence of the turbines on the surface sensible heat flux, although in Fig. 4l we notice a few observations with slightly larger heating at NLAE 4 (up to 40 W m^{-2}) for south-southeasterly flow. Future CWEX experiments will sample surface heat fluxes deeper in the wind farm, where multiple wakes prevail, for comparison with those near the windward lines of turbines reported herein, where single wakes and gaps between wakes are more prevalent.

The CWEX-11 results showed similar results for the southerly B2 wake observations (wind directions from 165° to 195°) and exhibited the same daytime speed reductions, nighttime accelerations, and increases in TKE. These data also revealed a decrease (increase) in daytime (nighttime) temperature and a modest increase in downward heat transport (25 W m^{-2}), especially at the northernmost flux station (NCAR 4). However, the nighttime heat flux at NCAR 4

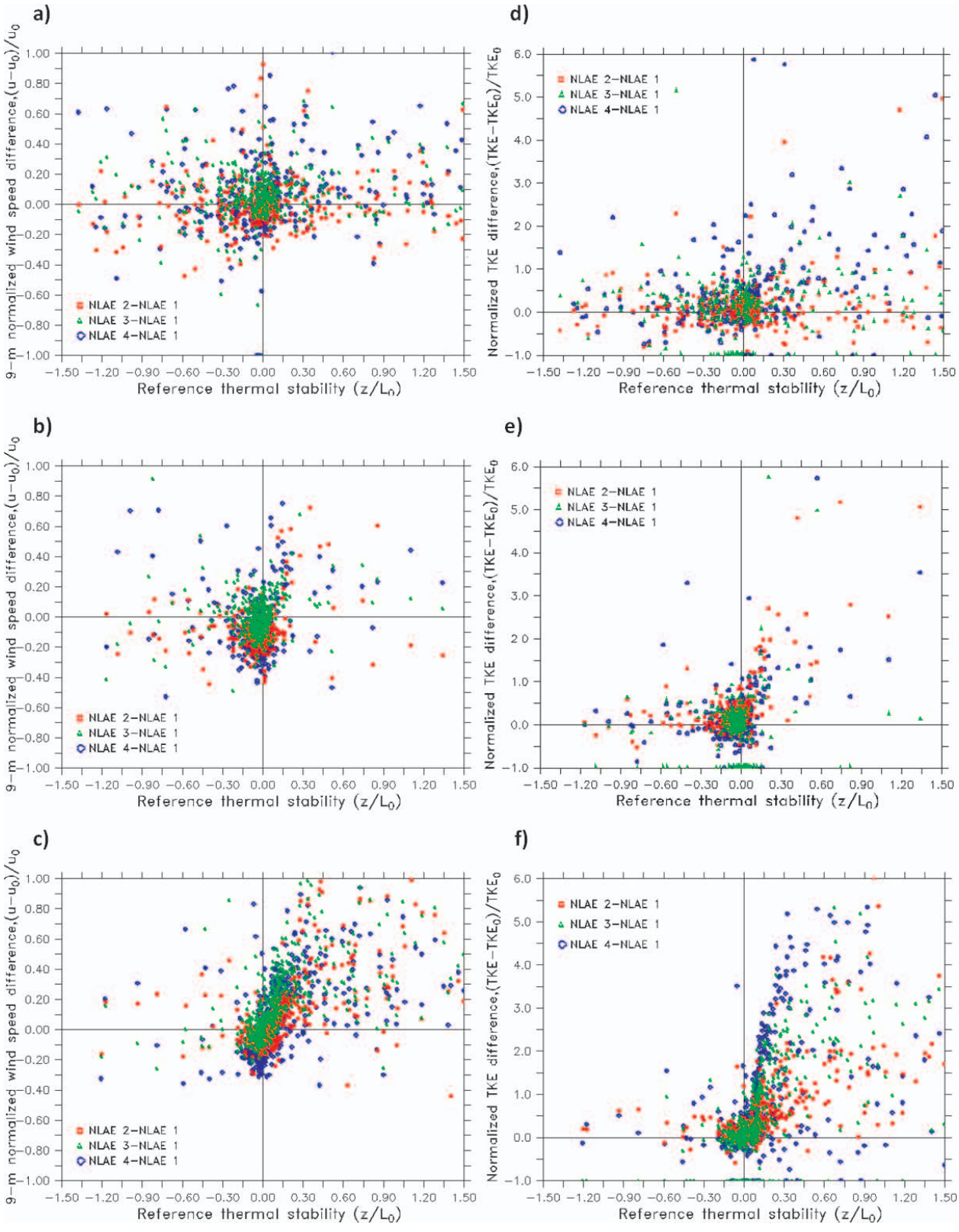

FIG. 4 (FACING PAGES). CWEX-10 differences (downwind – upwind) of normalized wind speed and normalized TKE, 9-m air temperature, and uncorrected sensible heat flux as functions of upwind flux tower thermal stability (z/L_0) for (a),(d),(g),(j) the westerly no-wake case; (b),(e),(h),(k) the SW B2 turbine wake case; and (c),(f),(i),(l) the SSE case between the wakes of turbines B2 and B3.

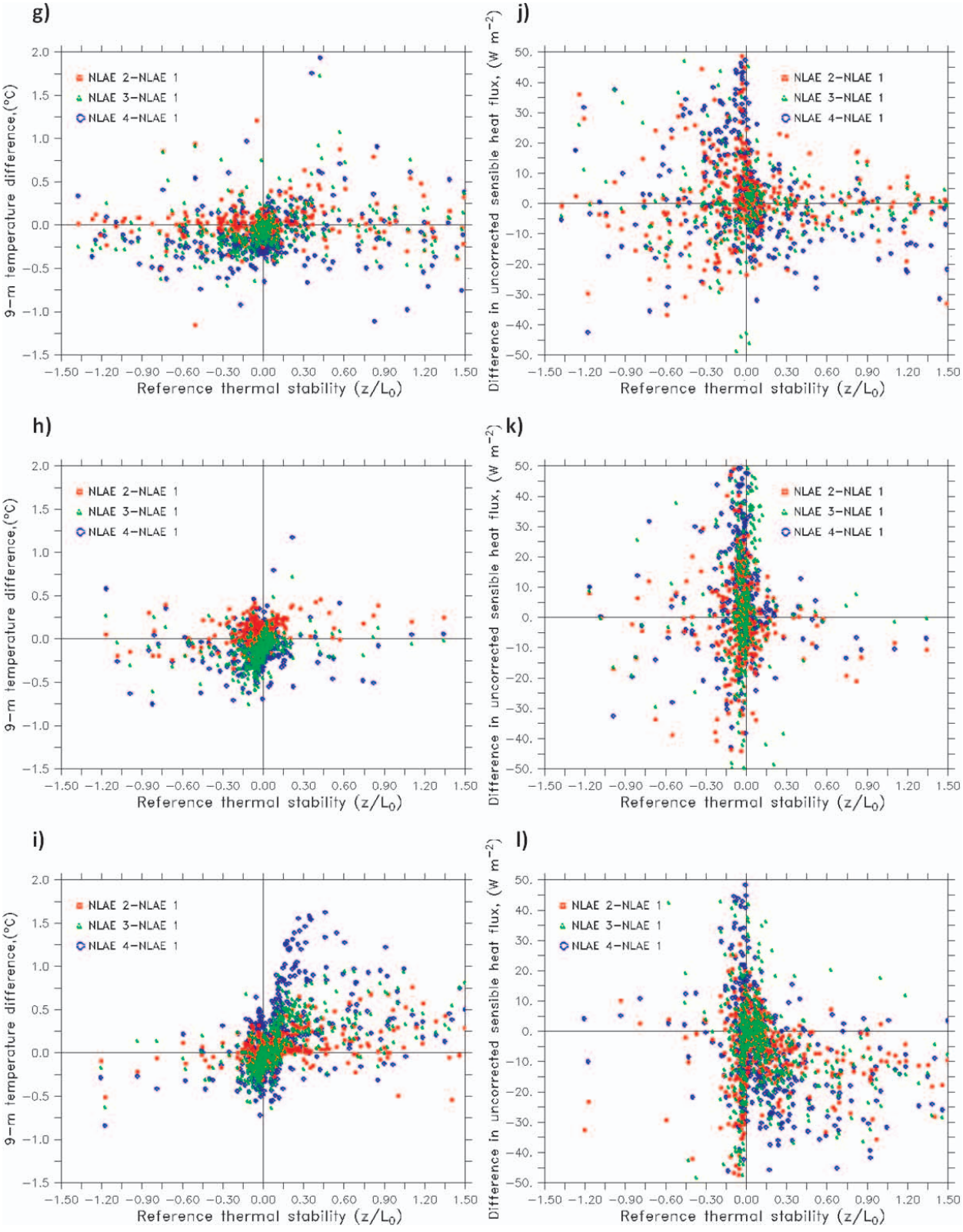
g)
j)
h)
k)
i)
l)
NLAE 2–NLAE 1
NLAE 3–NLAE 1
NLAE 4–NLAE 1
9–m temperature difference,(°C)
Difference in uncorrected sensible heat flux, (W m^{-2})
Reference thermal stability (z/L$_0$)
−1.50 −1.20 −0.90 −0.60 −0.30 0.00 0.30 0.60 0.90 1.20 1.50

Table 2. CWEX-10 means and standard deviations (in parentheses) of the differences (downwind – upwind) in normalized wind speed for upwind flux tower thermal stability (z/L_0) categories: unstable, neutral, and stable for the westerly no-wake case, the southwest B2 turbine wake case, and the south-southeast gap case between the wakes of turbines B2 and B3. Notable differences are indicated with an asterisk.

$\frac{\Delta U}{U_0}$		(NLAE 2 – NLAE 1)	(NLAE 3 – NLAE 1)	(NLAE 4 – NLAE 1)
No wake (west)	Unstable ($z/L_0 < -0.05$)	0.00 (0.24)	0.07 (0.18)	0.06 (0.28)
	Neutral ($-0.05 < z/L_0 < 0.05$)	0.03 (0.21)	0.06 (0.14)	0.02 (0.17)
	Stable ($z/L_0 > 0.05$)	0.02 (0.30)	0.10 (0.19)	0.16 (0.28)
B2 wake (southwest)	Unstable ($z/L_0 < -0.05$)	−0.10 (0.11)*	−0.01 (0.16)	−0.05 (0.32)
	Neutral ($-0.05 < z/L_0 < 0.05$)	−0.12 (0.08)*	−0.03 (0.09)	−0.13 (0.12)*
	Stable ($z/L_0 > 0.05$)	0.21 (0.56)	0.24 (0.34)	0.37 (0.84)
B2_B3 (south-southeast gap)	Unstable ($z/L_0 < -0.05$)	−0.01 (0.16)	0.01 (0.21)	−0.04 (0.28)
	Neutral ($-0.05 < z/L_0 < 0.05$)	−0.07 (0.06)*	0.01 (0.09)	−0.10 (0.12)*
	Stable ($z/L_0 > 0.05$)	0.16 (0.28)	0.31 (0.23)*	0.22 (0.25)*

Table 3. As in Table 2, but for normalized TKE.

$\frac{\Delta TKE}{TKE_0}$		(NLAE 2 – NLAE 1)	(NLAE 3 – NLAE 1)	(NLAE 4 – NLAE 1)
No wake (west)	Unstable ($z/L_0 < -0.05$)	0.05 (0.40)	0.26 (0.65)	0.21 (0.75)
	Neutral ($-0.05 < z/L_0 < 0.05$)	0.07 (0.23)	0.25 (0.34)	0.18 (0.42)
	Stable ($z/L_0 > 0.05$)	0.30 (1.08)	0.39 (0.66)	1.22 (1.98)
B2 wake (southwest)	Unstable ($z/L_0 < -0.05$)	0.12 (0.27)	−0.01 (0.79)	0.11 (0.51)
	Neutral ($-0.05 < z/L_0 < 0.05$)	0.12 (0.20)	0.06 (0.21)	0.03 (0.27)
	Stable ($z/L_0 > 0.05$)	2.68 (4.07)	1.89 (1.66)*	2.42 (2.37)*
B2_B3 (south-southeast gap)	Unstable ($z/L_0 < -0.05$)	0.13 (0.26)	−0.16 (1.03)	0.18 (0.62)
	Neutral ($-0.05 < z/L_0 < 0.05$)	0.09 (0.15)	0.06 (0.21)	0.05 (0.25)
	Stable ($z/L_0 > 0.05$)	1.07 (1.46)	1.34 (1.26)*	1.61 (1.69)*

Table 4. As in Table 2, but for 9-m air temperature.				
$\Delta T(C°)$		(NLAE 2 – NLAE 1)	(NLAE 3 – NLAE 1)	(NLAE 4 – NLAE 1)
No wake (west)	Unstable ($z/L_0 < -0.05$)	−0.11 (0.73)	−0.14 (0.24)	−0.20 (0.26)
	Neutral ($-0.05 < z/L_0 < 0.05$)	0.00 (0.49)	−0.05 (0.14)	−0.41 (2.04)
	Stable ($z/L_0 > 0.05$)	−0.02 (0.69)	0.01 (0.32)	−0.08 (0.42)
B2 wake (southwest)	Unstable ($z/L_0 < -0.05$)	0.06 (0.14)	−0.19 (0.19)*	−0.11 (0.22)
	Neutral ($-0.05 < z/L_0 < 0.05$)	−0.15 (1.29)	−0.13 (0.12)*	−0.08 (0.17)
	Stable ($z/L_0 > 0.05$)	−0.04 (1.42)	0.05 (0.24)	−0.02 (0.32)
B2_B3 (south-southeast gap)	Unstable ($z/L_0 < -0.05$)	−0.01 (0.14)	−0.14 (0.21)	−0.06 (0.27)
	Neutral ($-0.05 < z/L_0 < 0.05$)	0.04 (0.08)	−0.08 (0.12)	0.00 (0.19)
	Stable ($z/L_0 > 0.05$)	0.10 (0.24)	0.32 (0.25)*	0.43 (0.43)*

Table 5. As in Table 2, but for uncorrected sensible heat flux.				
$\Delta H(W\ m^{-2})$		(NLAE 2 – NLAE 1)	(NLAE 3 – NLAE 1)	(NLAE 4 – NLAE 1)
No wake (west)	Unstable ($z/L_0 < -0.05$)	0.13 (15.13)	−12.31 (43.68)	11.37 (25.90)
	Neutral ($-0.05 < z/L_0 < 0.05$)	5.40 (11.94)	−2.98 (18.94)	13.03 (23.64)
	Stable ($z/L_0 > 0.05$)	−0.34 (7.76)	−0.17 (6.18)	−5.93 (9.60)
B2 wake (southwest)	Unstable ($z/L_0 < -0.05$)	0.23 (17.94)	−0.89 (31.19)	14.74 (39.41)
	Neutral ($-0.05 < z/L_0 < 0.05$)	−0.08 (12.34)	6.99 (19.39)	10.98 (24.16)
	Stable ($z/L_0 > 0.05$)	−6.62 (17.04)	0.28 (23.58)	−1.08 (14.96)
B2_B3 (south-southeast gap)	Unstable ($z/L_0 < -0.05$)	−9.07 (19.16)	−18.28 (36.25)	18.30 (37.58)
	Neutral ($-0.05 < z/L_0 < 0.05$)	−3.02 (11.38)	−0.71 (19.18)	10.55 (27.10)
	Stable ($z/L_0 > 0.05$)	−6.06 (9.14)	−6.24 (14.04)	−11.31 (12.94)

(CWEX-11) was weaker than what was observed at the NLAE 4 (CWEX-10), which we attribute to the influence of wakes from multiple lines of turbines.

TURBINE WAKE INFLUENCES ON WIND AND TURBULENCE PROFILES: A CASE STUDY, NIGHT OF 16–17 JULY 2011. A case study is presented to show the coupling between wake aloft and surface processes. The overnight period of 16–17 July 2011 featured southerly flow within the wind farm during a convection-free and cloud-free period. The dewpoint depression was less than 2°C, but airport Automated Surface Observing System (ASOS) stations near the wind farm recorded visibilities of two to three standard nautical miles or greater (NCAR 2011). A synoptic-scale backing pattern was revealed in the flux station and lidar observations. The undisturbed wind profile (Fig. 5a) indicated winds steadily increasing with height, with a maximum between 12 and 14 m s^{-1} at 220 m above the surface, and this persisted throughout the night. The wake characteristics in Fig. 5c can be quantified by subtracting the downwind observations (Fig. 5b) from the upwind observations. The momentum

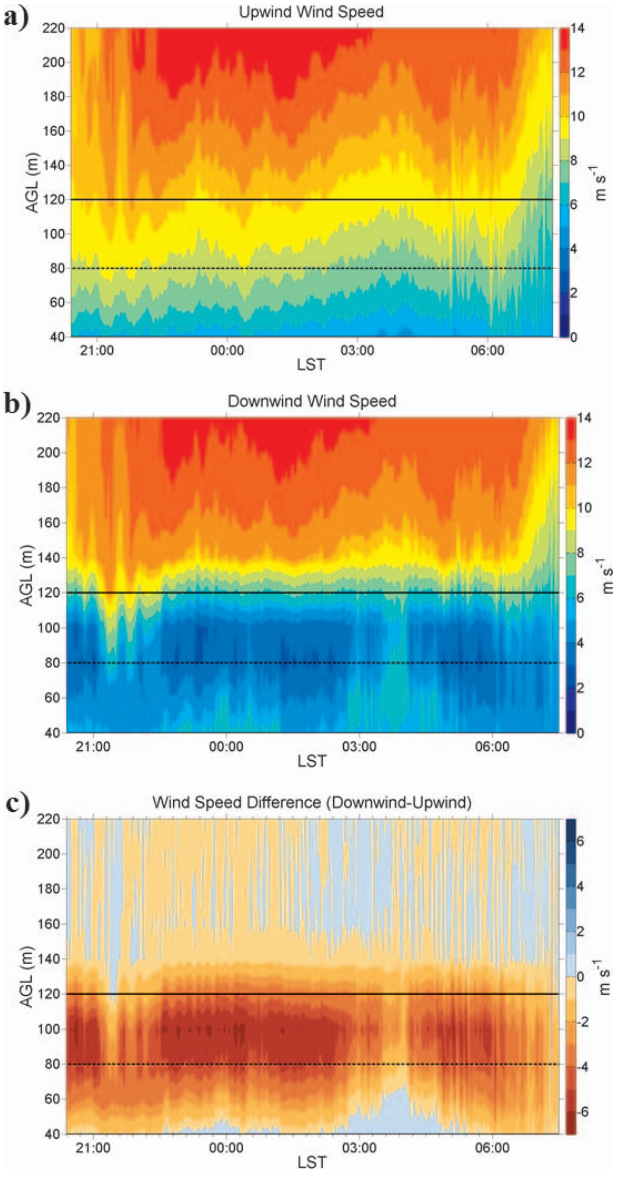

FIG. 5. Contours of wind speed from (a) WC 68, (b) WC 49, and (c) calculated difference in wind speed attributed to the wind turbine wake effect. Overlay with a solid black line is for the top of the rotor height, and the dashed black line indicates the hub height.

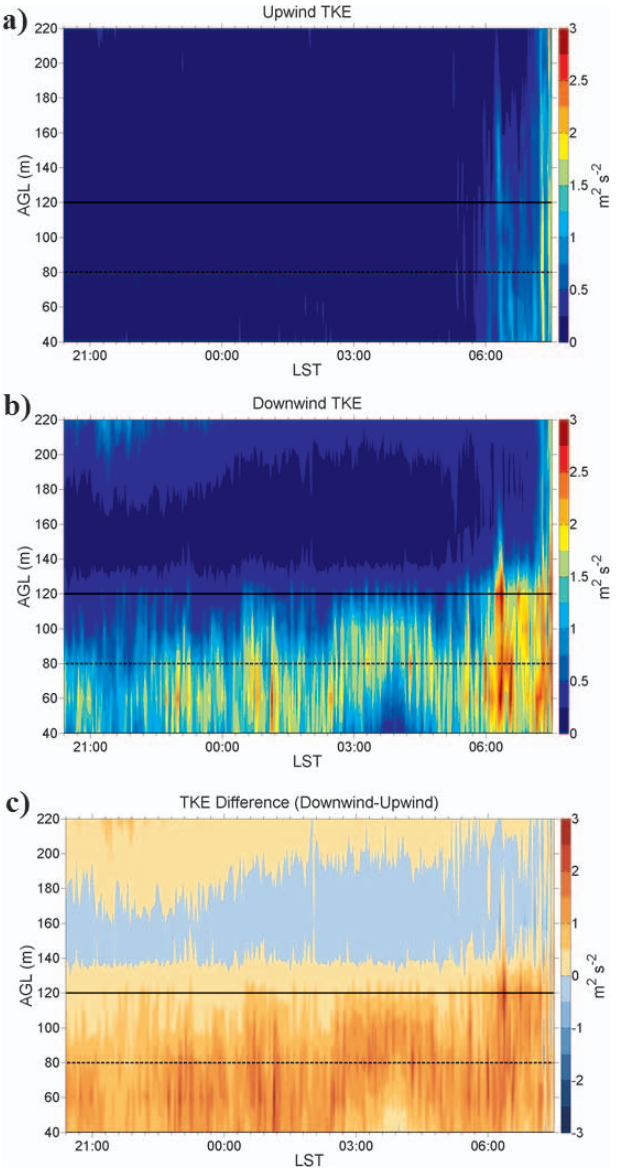

FIG. 6. Time–height cross sections of (a) upwind TKE profile, (b) downwind TKE profile, and (c) difference between (a) and (b). Overlay with a solid black line is for the top of the rotor height, and the dashed black line indicates the hub height.

deficit of the wake occurs in the layer of the turbine rotor disk (40–120 m), with some expansion in the vertical to 140 m. The largest wake deficits of ~6 m s^{-1} occurred at 100 m (which is above the 80-m hub height) and represent a speed decrease of 40%. The lowest level of Windcube observations, 40 m above the surface, suggests some slight acceleration below the wake, but these wind speed differences were small, being less than 1 m s^{-1}.

The standard deviations of velocities measured by the lidar are used to estimate TKE using the following relationship:

$$\mathrm{TKE}_{\mathrm{lidar}} = \frac{1}{2}(\sigma_u^2 + \sigma_v^2 + \sigma_w^2),$$

where σ_u, $\sigma_{u,}$ and $\sigma_{w,}$ represent the standard deviations of the zonal, meridional, and vertical wind components, respectively. Some reports have indicated disagreement between lidar turbulence metrics and those from in situ instruments (Sathe et al. 2011); however, the purpose herein is a comparison of two lidar measurements, not a strict calculation of TKE at one location per se. Upwind, downwind, and difference time–height cross sections of lidar estimates of TKE (Fig. 6) corroborate previous studies (Högström et al. 1988, among others) showing TKE increases in the wake. We observed that TKE enhancement was confined to the turbine rotor disk layer during the night, with some lofting occurring after sunrise as convective eddies lifted from the surface. In the midmorning through early afternoon, there is a slight expansion of turbine turbulence to about 20 m above the rotor layer. We expect a sharp decrease of turbulence above the rotor layer during the night as the temperature stratification prevents vertical mixing of these larger eddies and sustains the ambient "upwind" turbulence above the turbines.

Wake effects were also revealed in the 15-min averages of the surface fluxes. As found in CWEX-10, the region below the wake experiences significant overspeeding (0.5–1.0 m s^{-1}), not only at the near-wake location (NCAR 2), but also at the far-wake tower (NCAR 4). Data from the ISU flux towers located between turbine wakes exhibit less overspeeding than from the flux stations directly downwind of turbine B2 (Fig. 7a). We present differences in the data from two ISU towers and the reference NCAR tower, but we caution that the differences in measurement height (8 vs 10 m) are responsible for the higher speeds for the NCAR sites. Wake effects on TKE show a similar pattern (Fig. 7b): the NCAR flux stations directly north of turbine B2 exhibit TKE enhancements of as much as 0.30 m^2 s^{-2}, whereas there is negligible difference in turbulence between the two stations in the gap region (ISU 2 – ISU 1) when wind directions are between 170° and 180°. However, for the wind direction near 160°, the turbulence at ISU 2 increases because the edge of the B3 wake has shifted over the flux tower; conversely, the turbulence is reduced at the NCAR stations north of turbine B2 because the edge of the wake has moved to the left of the line of the NCAR flux stations.

We observe a slightly larger difference in 10-m temperature (0.3°C) between the gap stations (Fig. 7c), whereas the NCAR stations do not report any significant warming downstream of turbine B2. However, for the 4.5-m sonic temperature (figure not shown), there is roughly a 0.5°C difference between NCAR 4 and NCAR 1, with lower contrasts (0.25–0.4°C) between the upwind flux tower and the near-wake (NCAR 2) or intermediate location (NCAR 3). The 4.5-m temperature difference in the gap region is the smallest of any plotted (±0.1°C), being about 0.25°C higher downwind only when a wind direction from 160° from 0330 to 0500 LST positions the edge of the wake over the ISU 2 flux station. Measurements of sensible heat flux in far-wake locations (NCAR 3–4) show (Fig. 7d) a larger downward heat flux by 15–20 W m^{-2} as compared to the enhancement at the near-wake position (NCAR 2). For periods with flow slightly oblique to the tower line (near 160°), the heat flux difference between NCAR 2 and NCAR 1 is reduced, whereas the ISU 2–ISU 1 difference indicates more downward heat transport within the B3 wake above the ISU station.

We conclude that, for this southerly wind case, the turbine wakes from B2 and B3 are confined to an approximately 5° expansion and do not impact the "gap" stations (ISU 1 and ISU 2). Further, the overspeeding and enhancement of TKE at NCAR 4 are near the magnitudes observed at NCAR 2, but the effect is less noticeable at NCAR 3. Perhaps this is an indication that the turbine wake reaches the surface beyond 10*D* downstream of an individual turbine for this nighttime case.

Interpretation of observed winds and TKE near the turbine line calls for a more refined conceptual model of the pressure field, which we adopt from our previous modeling and measurements around agricultural shelterbelts (Wang et al. 2001). The turbines present a barrier to the flow, which creates a stationary (assuming a constant wind speed and wind direction) perturbation pressure field at the surface, with high pressure upwind and low pressure downwind. The largest increases in speed and turbulence behind the turbines occur at NCAR 2, which is consistent with a

perturbation–pressure-driven speedup immediately behind the turbine. The overspeeding and the reduction of TKE at the ISU 2 flux tower between turbines B2 and B3 suggests that the differences in wind speed are also forced by the perturbation pressure fields around each turbine. Our results suggest a need for future exploration of the perturbation pressure and flow effects around individual turbines and around multiple lines of wind turbines.

TURBINE INFLUENCES ON FLUXES OF HEAT AND CARBON DIOXIDE. Exchanges of CO_2, moisture, and heat between atmosphere and crops have important agricultural, as well as microclimate and mesoscale flow, consequences. Figure 8 provides a contrast between the 30-min-average fluxes of sensible and latent heat and the carbon dioxide for the daytime southwesterly flow case of 18 July 2011 and the daytime frontal case of 2 August 2011. The Webb–Pearman–Leuning correction (Webb et al. 1980) was applied to the latent heat and CO_2 fluxes. Skies were generally clear in both cases except for a period of cloudiness from 1250 to 1345 LST 2 August (delineated by the vertical dashed lines in Figs. 8b,d,f). The sensible heat flux difference between NCAR 3 and NCAR 1 is slightly larger on 2 August compared to 18 July but neither showed large change over the course of the day (Figs. 8a,b). Downwind–upwind latent heat flux differences for the two days (Figs. 8c,d) are similar in the morning hours. After the cloudiness period on 2 August, the NCAR 3–NCAR 1 difference in the latent heat flux suggests a sign reversal, which is in contrast to a positive mean value for the afternoon of 18 July. The vertical flux differences of carbon dioxide (Figs. 8e,f) are similar in the morning with higher downward flux downwind of the turbines. In the afternoon (after the period of cloudiness on 2 August) the fluxes are essentially identical on 2 August, whereas for 18 July the morning pattern is preserved. These data show that changes in relative magnitude of the latent heat flux and CO_2 flux take place at the same time as

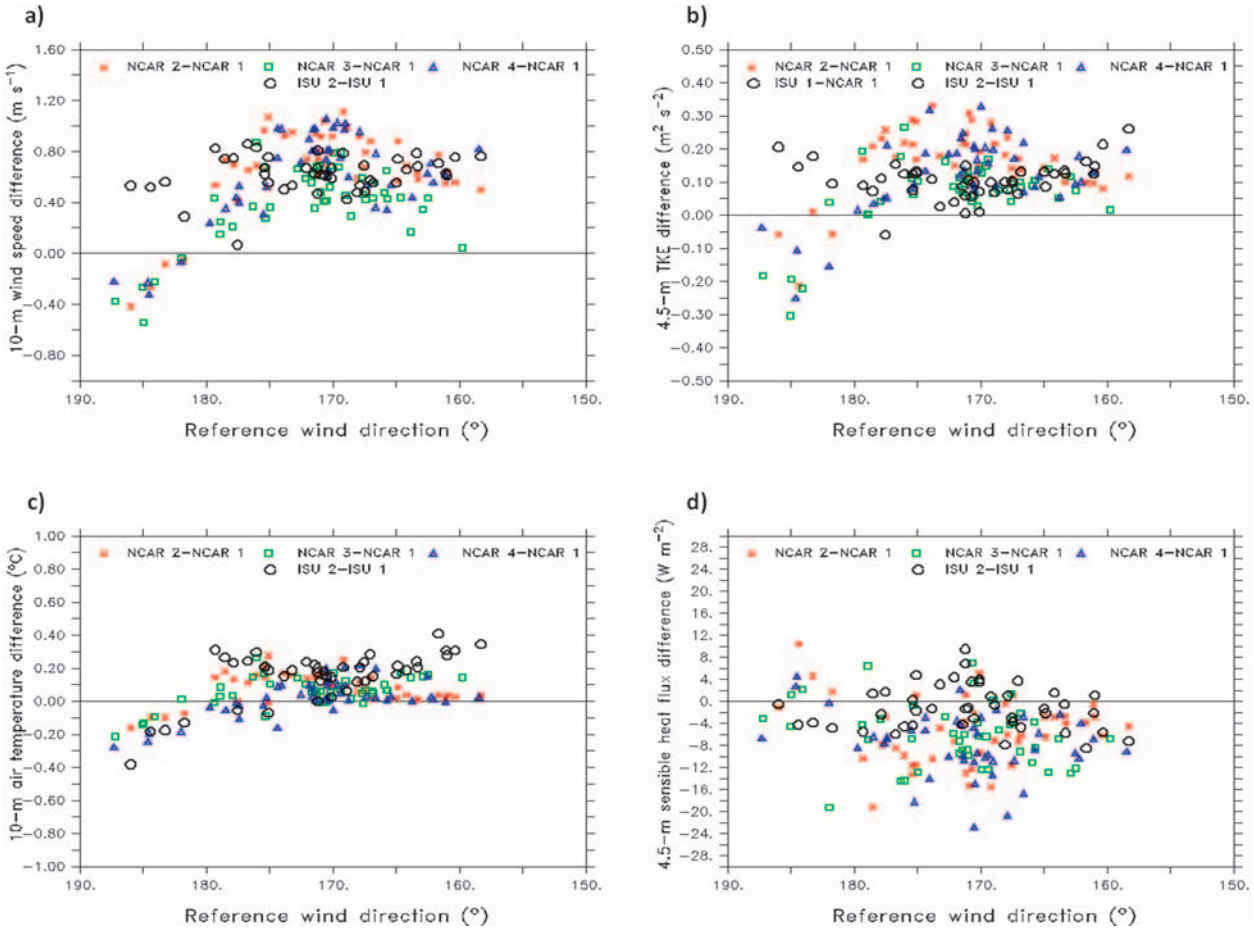

FIG. 7. Differences during the night of 16–17 Jul 2011 for (a) wind speed (b) TKE, (c) air temperature, and (d) sensible heat flux. Note that at the ISU tower, wind speed and temperature are collected at the 8-m level, while the NCAR tower wind speed and temperature are observed at 10 m.

the change in wind direction. These are consistent with (but perhaps not proof of) turbines creating an increase in upward latent heat flux and downward CO_2 flux over the crop during the daytime.

REMAINING SCIENCE QUESTIONS AND FUTURE CAMPAIGNS. CWEX-10/CWEX-11 provided evidence of changes in flow structures around single turbines or single lines of turbines,

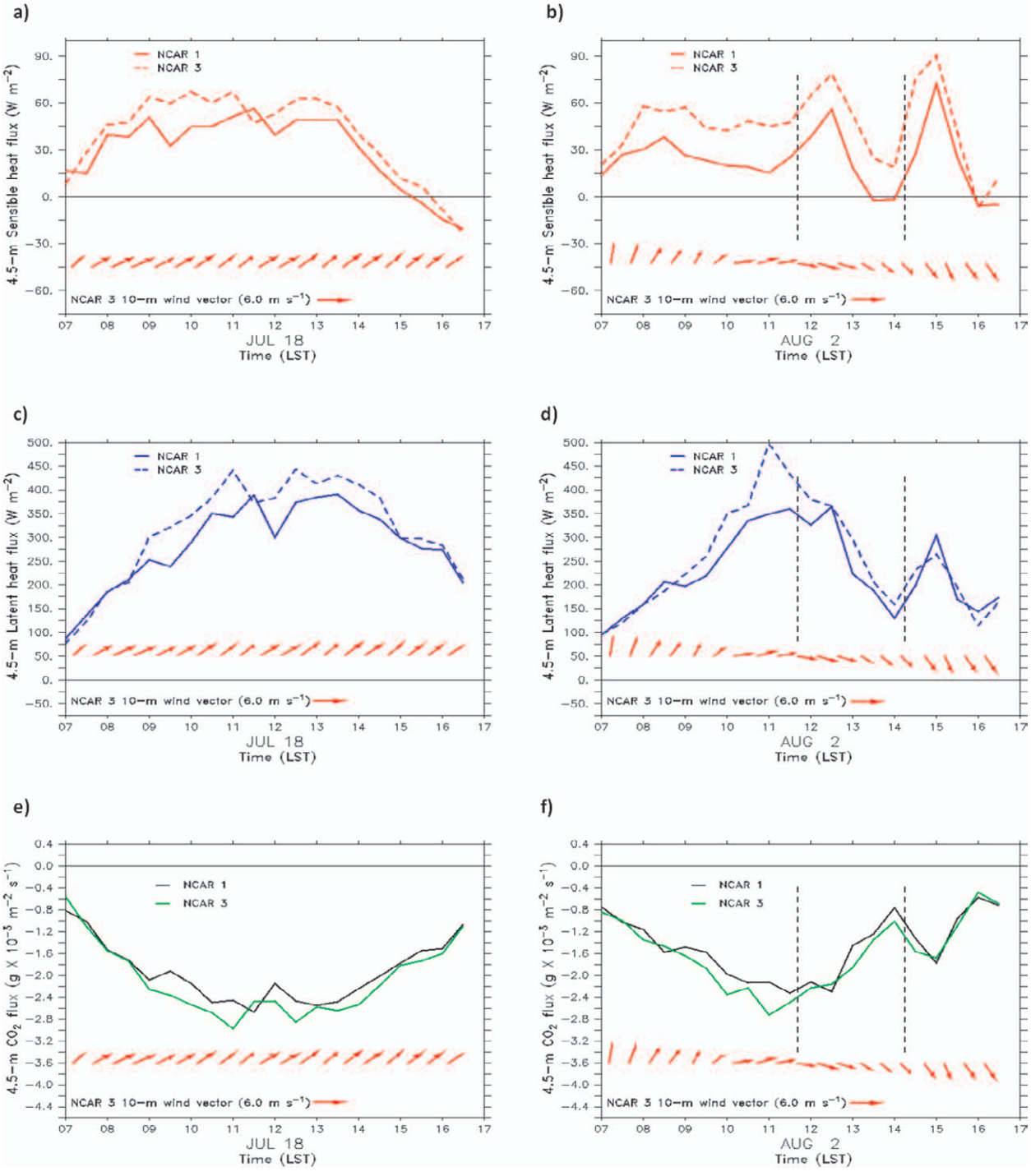

Fig. 8. Comparison of differences in 30-min-averaged fluxes of (a),(b) sensible heat, (c),(d) latent heat, and (e),(f) CO_2 between NCAR 3 and NCAR 1 for a southerly wind case on 18 Jul 2011 and for a transition from a southerly to a northwesterly direction on 2 Aug 2011. NCAR 3 10-m wind direction vectors are overlaid for each image. Dashed lines in (b),(d),(f) denote the period of cloudiness during the transition of winds from southerly to northwesterly on the early afternoon of 2 Aug 2011.

and evidence suggesting turbines modify fluxes of importance to crops (e.g., heat and CO_2). Our analysis of these data, together with our previous experience from modeling and measurements of the aerodynamics of agricultural shelterbelts (Wang et al. 2001), lead us to propose three mechanisms that influence surface micrometeorological conditions in the near lee of turbines: 1) wind turbine wakes overhead that have not reached the surface but modify the wind profile, scales of turbulence, and the vertical mixing between the surface and the overlying boundary layer; 2) wind turbine wakes that are intersecting the surface, allowing wake turbulence to modify the surface microclimate; and 3) static pressure fields (high pressure upwind and low pressure downwind) around each turbine and line of turbines that generate perturbations in surface flow (e.g., localized over speeding) and fluxes within a few diameters of the turbine line. Additional analyses of CWEX-10/CWEX-11 data and future CWEX experiments to map out the pressure fields will further explore these proposed mechanisms.

The experiments thus far do not provide measurements of plant growth and yield influences of turbines (addressing questions 2–4). CWEX-10/CWEX-11 demonstrated that turbines very likely have positive (e.g., enhanced daytime CO_2 flux down into the crop canopy) and negative (e.g., higher nighttime temperature, which enhances respiration) effects over short periods. However, variability within and between fields due to cultivar, soil texture and moisture content, and management techniques creates large uncertainties for attributing season-long biophysical changes, and much less yield, to turbines alone. A caveat to this statement is that we have not sampled the center of the wind farm, where aggregate effects of multiple rows of turbines may be more pronounced. Enlarging the study domain would allow this and other agronomic questions to be addressed. For instance, staging an intensive observation period during the corn pollination period (mid-July to early August) offers a unique opportunity to study the transport and viability of pollen throughout the atmospheric boundary layer. In addition to conducting biophysical studies of pollen, this experiment could use pollen as a passive tracer for studying mesoscale influences of the wind farm (see the discussion below).

There is additional motivation for studying the impact of the wind farm as a whole as a basic science question, in addition to informing future siting and operation of wind farms. For instance, better understanding is needed on how the mean and turbulent flow fields of the turbine layer interact with the overlying boundary layer and how this changes from day to night when (at least in summer in the central United States) a strong low-level jet becomes established with peak winds within a few hundred meters of the surface. Additional unknowns relate to mesoscale influences on the flow fields around and over the wind farm, which has an area of about 150 km^2. What are the impacts on low-level ($z < 100$ m) convergence patterns around the wind farm and vertical velocities above or downwind of the wind farm at 200 m, 500 m, and top of the boundary layer? Do they correspond with the impacts suggested by wind farm parameterizations in mesoscale models (Baidya Roy et al. 2004; Barrie and Kirk-Davidoff 2010; Baidya Roy 2011; Fitch et al. 2012)? Are these changes in convergence patterns sufficient to change patterns of boundary layer clouds [e.g., via gravity wave formation in wind farms described by Smith (2010)]? Are the resulting magnitudes of changes sufficient to reorganize convectively driven systems, leading to precipitation (Fiedler and Bukovsky 2011) or to change nonconvective forcing of precipitation [e.g., isentropic lift, conditional symmetric instability (CSI), and mesoscale banding]? Effects of mesoscale terrain, such as the Loess Hills feature along the Iowa side of the Missouri River, which can generate a very shallow short-wave train close to the surface, could potentially interact with wind farm dynamics. The activity of this shallow short-wave train may lead to the fluctuation of surface winds across the wind farm under stable nighttime flow.

Finally, numerical modeling using large-eddy simulation (LES) and other high-resolution models is needed to explore how a wind farm interacts with ambient meteorological conditions to create local winds, transports, and stresses on wind turbine components. A deeper understanding of these interactions is needed for improved forecasts of wind power output by individual turbines within the wind farm, and the forces and stresses (possibly leading to blade and gearbox damage) likely to accrue from spatial and temporal changes in turbulence patterns. Databases of field measurements from operating wind farms are needed to validate a variety of wind tunnel and numerical simulation models (Chamorro and Porté-Agel 2009; Calaf et al. 2010; Churchfield et al. 2010; Cal et al. 2011; Lu and Porté-Agel 2011; Porté-Agel et al. 2011; Churchfield et al. 2012).

Current plans call for erection of two 120-m towers in the vicinity of the wind farm for additional vertical measurements in future CWEX experiments. A community call is planned to invite participation of other measurement teams for an expanded field program in the summer of 2014 that will address the many science

and application questions we have raised. NCAR data from CWEX-11 are available from the CWEX-11 data archive website of the Earth Observing Laboratory of NCAR (www.eol.ucar.edu/deployment/educational-deployments/CWEX11). Other data from CWEX-10 and CWEX-11 will be become available in the near future from the Iowa Environmental Mesonet (http://mesonet.agron.iastate.edu/index.phtml). Researchers interested in joining future CWEX experiments should contact coauthor E. S. Takle.

ACKNOWLEDGMENTS. This work was supported in part by the National Renewable Energy Laboratory under Professor Lundquist's joint appointment. NREL is a national laboratory of the U.S. Department of Energy, Office of Energy Efficiency and Renewable Energy, operated by the Alliance for Sustainable Energy, LLC. Partial funding for CWEX-10 was provided by the Ames Laboratory (DOE) and the Center for Global and Regional Environmental Research at the University of Iowa. Surface flux stations for CWEX-11 were provided by the NCAR Earth Observing Laboratory under an instrumentation deployment, and undergraduate student participation was supplemented by funding from an NSF REU program under Grant 1063048. Data analysis was supported in part by the National Science Foundation under the state of Iowa EPSCoR Grant 1101284.

REFERENCES

Aitken, M. L., M. E. Rhodes, and J. K. Lundquist, 2012: Performance of a wind-profiling lidar in the region of wind turbine rotor disks. *J. Atmos. Oceanic Technol.,* **29,** 347–355, doi:10.1175/JTECH-D-11-00033.1.

AWEA, cited 2011: U.S. wind industry year-end 2010 market report. [Available online at www.awea.org/learnabout/publications/upload/4Q10_market_outlook_public.pdf.]

Baidya Roy, S., 2011: Simulating impacts of wind farms on local hydrometeorology. *J. Wind Eng. Ind. Aerodyn.,* **99,** 491–498, doi:10.1016/j.jweia.2010.12.013.

——, and J. J. Traiteur, 2010: Impacts of wind farms on surface temperatures. *Proc. Natl. Acad. Sci. USA,* **107,** 17899–17904, doi:10.1073/pnas.1000493107.

——, S. W. Pacala, and R. L. Walko, 2004: Can large wind farms affect local meteorology? *J. Geophys. Res.,* **109,** D19101, doi:10.1029/2004JD004763.

Barrie, D. B., and D. B. Kirk-Davidoff, 2010: Weather response to a large wind turbine array. *Atmos. Chem. Phys.,* **10,** 769–775, doi:10.5194/acp-10-769-2010.

Barthelmie, R. J., and Coauthors, 2010: Quantifying the impact of wind turbine wakes on power output at offshore wind farms. *J. Atmos. Oceanic Technol.,* **27,** 1302–1317, doi:10.1175/2010JTECHA1398.1.

Cal, R. B., J. Lebrón, L. Castillo, H. S. Kang, and C. Meneveau, 2011: Experimental study of the horizontally averaged flow structure in a model wind-turbine array boundary layer. *J. Renewable Sustainable Energy,* **2,** 013106, doi:10.1063/1.3289735.

Calaf, M., C. Meneveau, and J. Meyers, 2010: Large eddy simulation study of fully developed wind-turbine array boundary layers. *Phys. Fluids,* **22,** 015110, doi:10.1063/1.3291077.

Campbell, G. S., and J. M. Norman, 1998: *An Introduction to Environmental Biophysics.* 2nd ed. Springer–Verlag, 286 pp.

Chamorro, L. P., and F. Porté-Agel, 2009: A wind-tunnel investigation of wind-turbine wakes: Boundary-layer turbulence effects. *Bound.-Layer Meteor.,* **132,** 129–149, doi:10.1007/s10546-009-9380-8.

Churchfield, M. J., G. Vijayakumar, J. G. Brasseur, and P. J. Moriarty, 2010: Wind energy-related atmospheric boundary layer large-eddy simulation using OpenFOAM. Preprints, *19th Symp. on Boundary Layers and Turbulence,* Keystone, CO, Amer. Meteor. Soc., 1B.6. [Available online at https://ams.confex.com/ams/19Ag19BLT9Urban/techprogram/paper_172636.htm.]

——, S. Lee, J. Michalakes, and P. J. Moriarty, 2012: A numerical study of the effects of atmospheric and wake turbulence on wind turbine dynamics. *J. Turbul.,* **13,** doi:10.1080/14685248.2012.668191.

Fiedler, B. H., and M. S. Bukovsky, 2011: The effect of a giant wind farm on precipitation in a regional climate model. *Environ. Res. Lett.,* **6,** 045101, doi:10.1088/1748–9326/6/4/045101.

Fitch, A. C., J. B. Olson, J. K. Lundquist, J. Dudhia, A. K. Gupta, J. Michalakes, and I. Barstad, 2012: Local and mesoscale impacts of wind farms as parameterized in a mesoscale NWP model. *Mon. Wea. Rev.,* **140,** 3017–3038, doi:10.1175/MWR-D-11-00352.1.

General Electric Energy, cited 2009: 1.5 MW wind turbine. [Available online at www.ge-energy.com/wind.]

Högström, U., D. N. Asimakopoulos, H. Kambezidis, C. G. Helmis, and A. Smedman, 1988: A field study of the wake behind a 2 MW wind turbine. *Atmos. Environ.,* **22,** 803–820, doi:10.1016/0004–6981(88)90020-0.

Lu, H., and F. Porté-Agel, 2011: Large-eddy simulation of a very large wind farm in a stable atmospheric boundary layer. *Phys. Fluids,* **23,** 065101, doi:10.1063/1.3589857.

Magnusson, M., and A. S. Smedman, 1994: Influence of atmospheric stability on wind turbine wakes. *Wind Eng.,* **18,** 139–151.

Meyers, J., and C. Meneveau, 2012: Optimal turbine spacing in fully developed wind farm boundary layers. *Wind Energy,* **15,** 305–317, doi:10.1002/we.469.

NCAR, cited 2011: Image archive: Meteorological case study selection kit. [Available online at http://locust.mmm.ucar.edu.]

Porté-Agel, F., Y.-T. Wu, H. Lu, and R. J. Conzemius, 2011: Large-eddy simulation of atmospheric boundary layer flow through wind turbines and wind farms. *J. Wind Eng. Ind. Aerodyn.,* **99,** 154–168, doi:10.1016/j.jweia.2011.01.011.

Sathe, A., J. Mann, J. Gottschall, and M. S. Courtney, 2011: Can wind lidars measure turbulence? *J. Atmos. Oceanic Technol.,* **28,** 853–868, doi:10.1175/JTECH-D-10-05004.1.

Smith, R. B., 2010: Gravity wave effects on wind farm efficiency. *Wind Energy,* **13,** 449–458, doi:10.1002/we.366.

Stull, R., 1988: *An Introduction to Boundary Layer Meteorology.* Kluwer Academic Publishers, 666 pp.

UCS, cited 2011: Farming the wind: Wind power and agriculture. [Available online at www.ucsusa.org/clean_energy/technology_and_impacts/impacts/farming-the-wind-wind-power.html.]

USDA, cited 2012: Crop production 2011 summary. USDA Rep. 1057-7823, 95 pp. [Available online at www.usda.gov/nass/PUBS/TODAYRPT/cropan12.pdf.]

U.S. DOE, 2008: 20% wind energy by 2030: Increasing wind energy's contribution to U.S. electricity supply. NREL Rep. TP-500-41869, DOE/GO-102008-2567, 248 pp. [Available online at www.nrel.gov/docs/fy08osti/41869.pdf.]

Wang, H., and E. S. Takle, 1995: A numerical simulation of boundary-layer flows near shelterbelts. *Bound.-Layer. Meteor.,* **75,** 141–173.

——, ——, and J. Shen, 2001: Shelterbelts and windbreaks: Mathematical modeling and computer simulation of turbulent flows. *Annu. Rev. Fluid Mech.,* **33,** 549–586.

Webb, E. K., G. I. Pearman, and R. Leuning, 1980: Correction of flux measurements for density effects due to heat and water vapor transfer. *Quart. J. Roy. Meteor. Soc.,* **106,** 85–100.